Facile synthesis of copper oxide nanoparticles using copper hydroxide by mechanochemical process

Heydar Khadivi Ayask[*], Jalil Vahdati Khaki, Mohsen Haddad Sabzevar

Department of Materials Science and Metallurgical Engineering, Engineering Faculty, Ferdowsi University of Mashhad,

Mashhad, Iran

Abstract

A facile mechanochemical-based method for synthesis of copper oxide (CuO) nanoparticles is here by introduced. For this purpose, copper hydroxide powder was synthesized through a facile solution method ($CuSO_4$ + 2 $Na(OH)$ → $Cu(OH)_2$ + Na_2SO_4) after which milling of as-prepared $Cu(OH)_2$ precursor and NaCl resulted in the mechanochemical dehydration of $Cu(OH)_2$ and dispersion of CuO nanoparticles into the salt matrix ($Cu(OH)_2$+2NaCl=$CuCl_2$+2NaOH and then $CuCl_2$+2NaOH=CuO+2NaCl+H_2O). Subsequently, washing the milled powders led to the removal of salt matrix and separation of CuO particles. The main advantages of the introduced method are synthesis of CuO nanoparticles with narrow size distribution without subsequent annealing during the process. The results of X-ray diffraction (XRD) indicated that the dehydration of $Cu(OH)_2$ into CuO was completed after three hours of milling. Structural analysis using scanning electron microscopy (SEM) equipped with energy dispersive spectroscopy (EDS), transmission electron microscopy (TEM) and particle size analyzer (PSA) showed that CuO particles had moderately equiaxed shape with sizes ranging from 10-27 nm. Also, the results of UV–visible absorption spectroscopy indicated that CuO nanoparticles had a band gap of 2.5 eV.

Keywords: *mechanochemical, nanostructure, visible and ultraviolet spectrometers, TEM.*

1. Introduction

Copper oxide (CuO) nanoparticles are under attention because of their unique thermal and mechanical properties as well as excellent optical and electrical performances. CuO nanoparticles exhibit a narrow band gap of about 1.2–1.9 eV. Particularly, their electrical properties can be affected by their quantum size leading to generation of p-type semiconductor. Due to the aforementioned properties, copper oxide (CuO) nanoparticles have found many applications in lithium ion batteries, gas sensors, high-Tc superconductors, antimicrobial agents and hydrogen detection [1-5].

During the past few years, variety of methods have been developed for the synthesis of such nanoparticles such as hydrothermal synthesis [1], sonochemical synthesis [4], colloid-thermal synthesis [5], microwave irradiation [6] and reverse micelle [7]. These are some of the chemical-based methods used for synthesis of copper oxide nanostructures with different morphologies of nanoparticles, nanoplatelets, nanoleaflets or nanowires. Generally, most of these methods involve multiple steps of $Cu(OH)_2$ fabrication as a sacrificial template followed by its thermal decomposition (Eq. 1) [8-10]:

$$Cu\,(OH\,)_2 \rightarrow\, CuO\, +\, H_2O_{(g)} \tag{1}$$
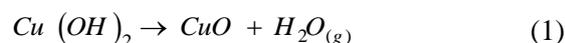
However, the applications of some of these chemical-based methods in industrial scale are limited due to agglomeration problems, non-uniform size distribution, low yields and high costs [11-13].

Thus, this article introduces a mechanochemical-based method for synthesis of CuO nanoparticles. Based on the literature,

synthesis of CuO nanoparticles by mechanochemical approach has not been reported yet. The key of this method is milling the precursors in a salt matrix and subsequently washing the powders to remove salt media. On the other hand, by mechanochemical synthesis two approaches for dispersion of nanoparticles within a salt matrix can be applied; 1) Solid-state chemical displacement reaction and; 2) milling process for the activation or disintegration of a precursor and within an inert salt matrix [13-16]. To the best of our knowledge, synthesis of metal oxide nanoparticles by these two approaches need annealing after the milling and washing steps. The introduced method has the advantage of synthesizing CuO nanoparticles without subsequent annealing during the process.

2. Experimental Methods

The introduced method for mechanochemical synthesis of CuO nanoparticles involves three stages (Fig. 1).
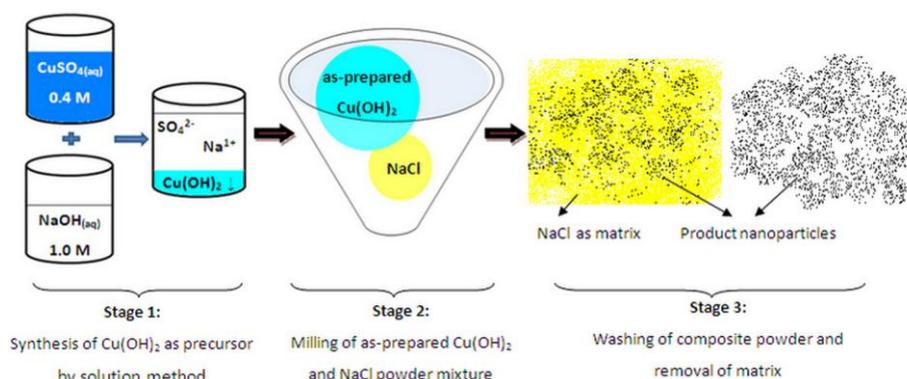
Fig. 1. Schematic of stages for mechanochemical synthesis of CuO nanoparticles

Stage 1- Synthesis of $Cu(OH)_2$ powder as a precursor by solution method: According to Eq. 2, a solution consisting 60 ml of NaOH (1M) is mixed with 75 ml of $CuSO_4$ (0.4 M) solution by stirring slowly at room temperature.

$$CuSO_{4\,(aq)} + 2Na\,(OH\,)_{(aq)} \rightarrow Cu\,(OH\,)_2 \downarrow$$
$$+Na_2SO_{4\,(aq)} \tag{2}$$
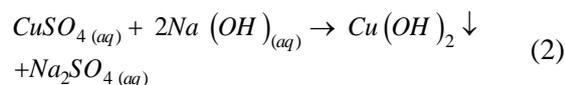
After 5 min of stirring the mixed solution, the resultant $Cu(OH)_2$ blue precipitate was filtered, washed with distilled water for

several times and dried at room temperature for 24 h.

Stage 2 Milling the as-prepared $Cu(OH)_2$ and NaCl powder mixture: $Cu(OH)_2$ and NaCl powders were mixed according to stoichiometric ratios (Eq. 3, 4).

$$7/2Cu\,(OH\,)_2 + 7NaCl = 7/2CuCl_2$$
$$+7NaOH \tag{3}$$

$$7/2CuCl_2 + 7NaOH = 7/2CuO + 7NaCl$$
$$+7/2H_2O \tag{4}$$
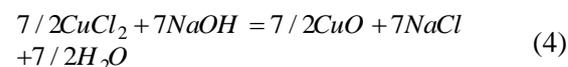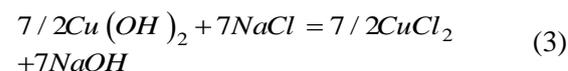
The mixture of starting powders were subjected to high energy planetary ball milling under the following conditions: The milling media was tool steel balls, ball to powder weight ratio (BPR) was 20:1 (with three different size of stainless steel balls), rotary velocity of the mill was 290 rpm, and milling times were 2, 3, 6 and 12 h. Experiments were performed at room temperature under atmospheric air.

Stage 3- Washing the composite powder and removal of matrix: Following the milling, the as-milled powders were washed several times with distilled water-ethanol solution in an ultrasonic bath and resultant products were recovered using centrifugation. Finally, washed powders were dried in air and at ambient temperature.

The phase identification of the powders was carried out with a Philips X'pert diffractometer with Cu Kα (λ= 1.54184 Å) radiation. The mean crystallite size of powders has been calculated using x-ray patterns and the Williamson-Hall method from the line broadening of the diffraction lines (Eq. 5) [17]:

$$B\cos\theta = 0.9\lambda / d + 2A\varepsilon Sin\theta \qquad (5)$$

where d is the average crystallite size (nm), λ is the Cu Kα wavelength (nm), β is the diffraction peak width at half maximum intensity (radian), and θ is the Bragg diffraction angle.

In order to determine the thermal properties of materials, differential thermal analyses such as (DTA) and thermogravimetric analyses (TGA) were performed using a STA503 (BAHR) instrument under atmospheric air at a heating rate 10°C/min.

The morphology of the resulting powders was studied by scanning electron microscopy (SEM- VP 1450) and transmission electron microscopy (TEM- Leo 912 AB). Also, a laser light scattering particle size analyzer (PSA, Cordouan-Vasco 3) was used to measure the particle size of powders.

Moreover, the ultraviolet (UV)–vis absorption spectrum of CuO suspension was measured using a UV–vis spectrophotometer (model Cecil, CE 8020).

It should be noted that the samples used for TEM, LLS and UV–vis characterization were dispersed in absolute ethanol and ultrasonicated for 10 min.

3. Results and discussion

3.1. Thermal analysis of Cu(OH)$_2$ precursor

As precursors, the blue color copper hydroxide precipitates was prepared from a reaction between CuSO$_4$ and NaOH solutions (Eq. 2). The XRD pattern of as-prepared copper hydroxide are presented in Figure 2. Compared with the standard XRD reference (JCPDS 35-0505), all the peaks can be indexed to orthorhombic Cu (OH)$_2$ as other materials have not been fabricated.

In order to thermally analyze the Cu(OH)$_2$ precursor, the results of DTA and TGA experiments as well as differential DTA (DDTA) and differential TGA (DTGA) curves are illustrated in Fig. 3. DTGA and DDTA curves confirmed the presence of one main step of weight loss in the TGA plot, and also one endothermic peak in the DTA plot of Cu (OH)$_2$ precursor.
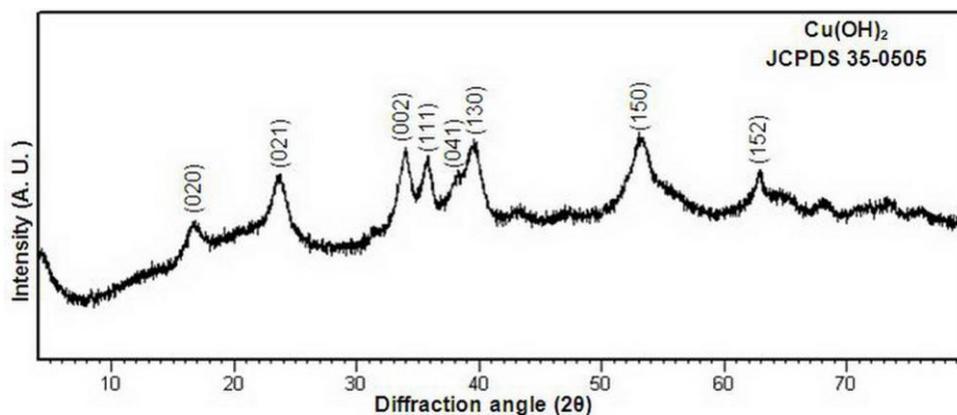
Fig. 2. XRD pattern of as-prepared Cu(OH)$_2$ powder synthesized via solution method
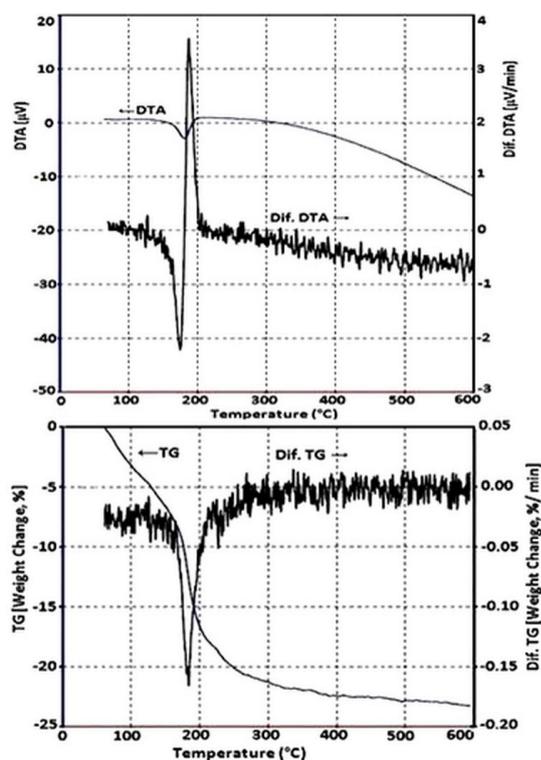
Fig. 3. DTA and TGA curves of as-prepared Cu(OH)$_2$

Fig. 4. XRD patterns of Cu(OH)$_2$+7NaCl starting materials (a) and milled-washed powders after milling time of 2 h (b), 3 h (c), 6 h (d), and 12 h (e)

According to DTA and DDTA curves, an evident endothermic peak was observed at approximately 180–200 °C. According to Eq. 1, this temperature range corresponds to the dehydration of Cu(OH)$_2$ and the formation of CuO [18]. Also, the TGA and DTG curves exhibited an apparent decrease in sample weight at temperatures ranging between 110–210°C. According to the DTG curve, weight loss of about 12% at this temperature range can be attributed to free water evaporation and Cu(OH)$_2$ dehydration.

3.2. Phase evaluation during mechanical milling of Cu(OH)$_2$ and NaCl

As a diluent material, NaCl is often used because of its inert nature and excellent milling ability. Moreover, incorporating an inert salt can prevent the growth of the synthesized nanoparticles, control particle size distribution and suppress their hard agglomeration [14-16, 19-21]. In the current research, NaCl is used as the diluent phase during mechanochemical synthesis of CuO nanoparticles from copper hydroxide.

Figure 4 shows the XRD patterns of Cu(OH)$_2$+7NaCl starting materials and milled-washed powders corresponding to different milling times of 2, 3, 6 and 12h.

As shown in Figure 4(a), the pattern of the as-mixed powders consist only the peaks of the two starting materials. However, for milled samples, according to Eq. 3 and 4, the peaks corresponding to the starting materials of Cu(OH)$_2$ and NaCl disappeared and new peaks corresponding to CuO were observed. However, no peaks of NaCl were identified in the milled-washed samples, indicating the successful removal of salt during the washing stage.

In the XRD pattern of 2 h milled sample (Fig. 4b), no sharp peaks showing the amorphous nature of CuO powders were observed. This is an interesting result as it indicates the beginning of a slow transformation to CuO. Finally, the transformation was completed after 3 h of milling and all CuO peaks appeared following washing of the as-milled mixture (Fig. 4c). The intensities and positions of the peaks are in good agreement with standard XRD reference (JCPDS 45-0937). In addition, no noticeable peaks such as Cu(OH)$_2$ or other copper compound were detected in this pattern, indicating the formation of single-phase CuO with a monoclinic structure. Furthermore, these results indicate that the dehydration of Cu(OH)$_2$ into CuO occurred

by mechanochemical process and not directly by thermal dehydration.

It is observed in Figure 4d that after 6 h of milling, the CuO peaks disappeared from the pattern and the peaks related to crystalline Cu_2O and Cu were identified. Figure 4e also shows that by increasing the milling time to 12h, Cu_2O peak intensity decreased while Cu peak intesity increased. Moreover new peaks related to Fe_2O_3 phase appeared in the of 12 h-milled sample pattern. The main reason for these phenomena can be justified by the role of Fe contamination as a reducing agent. As known, Fe contamination from the balls and the container increases with milling time[22-23], and this is one of the disadvantages of mechanical milling. Considering the role of Fe contamination, the following reactions (Eqs. 6 and 7) can be suggested as the main mechanisms for CuO removal and formation of Cu_2O, Cu and Fe_2O_3:

$$2CuO + (2/3) Fe \rightarrow Cu_2O + (1/3) Fe_2O_3$$
$$\Delta G^{0,298} \approx -129.418 \, kJ \qquad (6)$$

$$Cu_2O + (2/3) Fe \rightarrow 2Cu + (1/3) Fe_2O_3$$
$$\Delta G^{0,298} \approx -96.778 \, kJ \qquad (7)$$
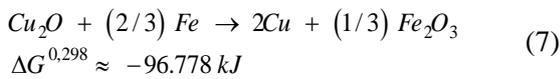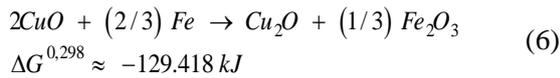
It should be noted that the role of Fe contaminations becomes more highlighted as milling time increases. In other words, Fe has no significant effect on the reduction process until 3 h of milling and acts as an impurity because of its very low amount. However due to increased Fe contamination at a higher milling time of 6 h, it acts as a reducing agent to reduce as-synthesized CuO to Cu_2O (Eq. 6) as well as Cu_2O to Cu (Eq. 7). As milling time increases to 12h, intensity of Cu_2O peaks decreased while the intensities of Cu and Fe_2O_3 peaks increases.

3.3. Structural analysis of CuO nanoparticles

As previously discussed 3h of milling is the optimum condition for mechanochemical synthesis of CuO powders. Peak broadening of CuO powders (Fig. 4c) indicates that CuO crystallite size is small. According to the Williamson-Hall equation (Eq. 5) the average crystallite size of the CuO nanoparticles is estimated to be 10.83 nm.

SEM micrographs and EDS analysis of CuO nanoparticles are illustrated in Figure 5. The EDS analysis was performed to investigate the elemental analysis of synthesized materials. As seen in Figure 5b, the EDS spectrum contains only Cu and O elements and no other elemental impurity such as Fe is detected. It confirmed the XRD results, that the final product is CuO powder free of any impurity.
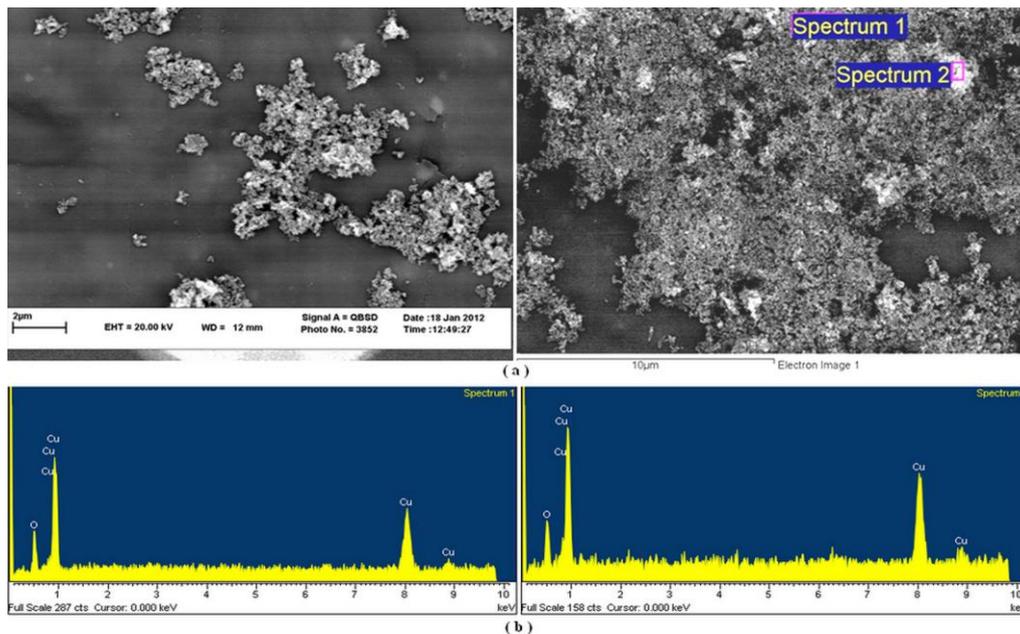
Fig. 5. a) SEM micrographs and b) EDS patterns of CuO powders

Figure 6 shows the bright field TEM image of washed CuO particles. As seen in this micrograph, CuO particles have moderately equiaxed shape and their sizes are in the range of 10-34 nm (average of 22 nm).

To investigate the size distribution of the CuO nanoparticles, a particle size histogram is presented in Figure7. According to LLS data, CuO nanoparticles have narrow size distribution and mean particle size of CuO nanoparticles is 27 nm.

Discussing mean particle size of as-synthesized CuO nanoparticles, Table 1 lists the crystallite size obtained from the XRD measurement and average particle size calculated from the TEM image and particle size analyzer.
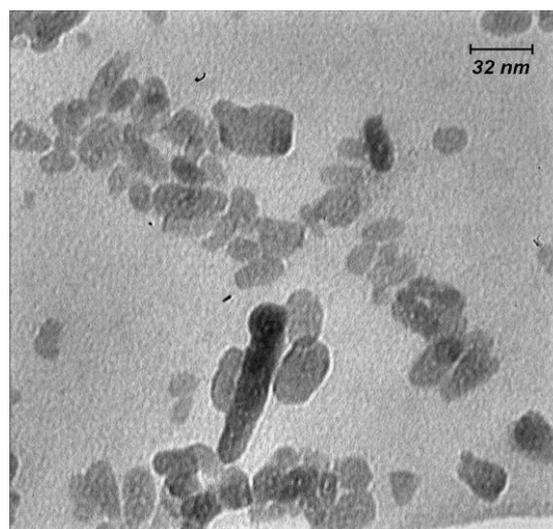
Fig. 6. TEM image of CuO nanoparticles
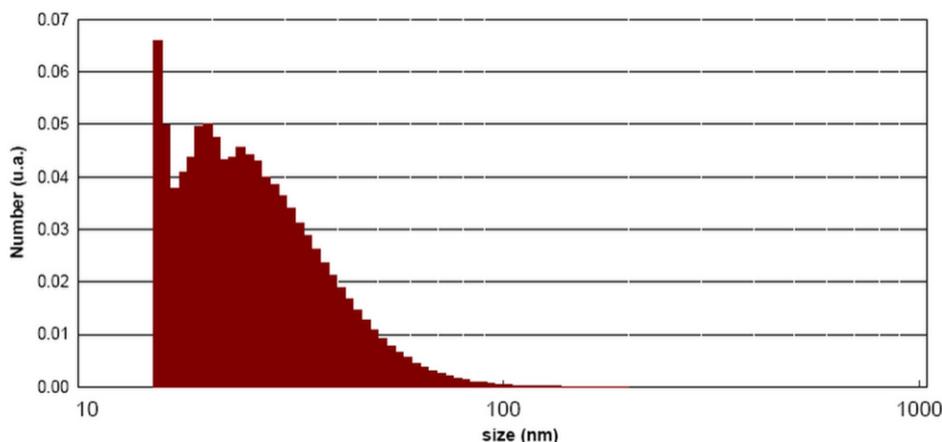
Fig. 7. Size distribution of the CuO nanoparticles

Table 1. Crystallite and average particle size of CuO nanoparticles

Sample	crystallite size, XRD (nm)	Particle size, TEM (nm)	Particle size, LLS (nm)
CuO nanopowder	10.83	22	27

According to Table 1, the particle size based on TEM image and particle size analyzer is larger than the crystallite size obtained by XRD peak broadening analysis. As known, the particles consist of aggregates of many primary crystals. Therefore, the apparent particle size is always larger than XRD crystallite size. Furthermore, this difference is due to the highly strained CuO resulting in X-ray peak broadening which

affects the crystallite size measured by the Williamson-Hall equation.

Microstructural refinement during mechanical dehydration can be vindicated by volumetric contraction ($\Delta V/V$) associated with the conversion of $Cu(OH)_2$ into CuO. The volumetric contraction ($\Delta V/V$) associated with the conversion of a molar equivalent volume of $Cu(OH)_2$ into CuO can be calculated by Eq. 8:

$$\frac{\Delta V}{V}(\%) = \frac{(\frac{M}{\rho})_{CuO} - (\frac{M}{\rho})_{Cu(OH)_2}}{(\frac{M}{\rho})_{Cu(OH)_2}} \times 100 \qquad (8)$$

The copper oxide is characterized by density of 6.32 g/cm^3 and molar mass of 80 g/mol, whereas $Cu(OH)_2$ has density of 3.37 g/cm^3 and molar mass of 98 g/mol. As a result, the conversion of a molar equivalent volume of $Cu(OH)_2$ into CuO would be associated with a volumetric contraction of approximately 56.45%.

3.4. UV–vis absorption analysis

Figure 8a shows the UV–Vis absorption spectrum of the synthesized CuO nanoparticles. The spectrum shows a broad absorption peak whose center is at about 390 nm. Light absorption leads to transmission of an electron into the conduction band and formation of a positive hole in the valence band. In small particles, they are confined to potential wells of small lateral dimension and the energy difference between the position of the conduction band and a free electron which leads to a quantization of their energy levels [2].
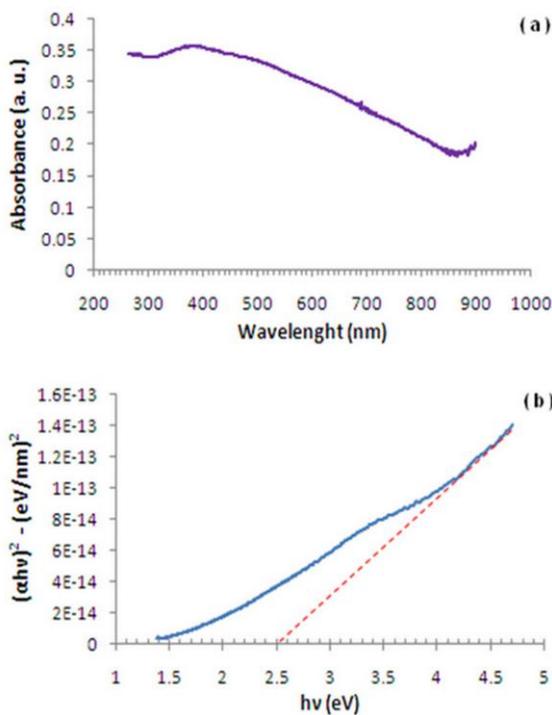
Fig. 8. a) UV–Vis the absorption spectrum of CuO nanoparticles, b) plot of $(\alpha h\nu)^2$ vs ($h\nu$); intersections of the dashed lines with the abscissa represents the band gap energy.

For semiconductor materials, the quantum confinement effect is expected if the semiconductor dimension becomes smaller than the Bohr radius of the excition, and so the absorption edge is shifted to a higher energy. The excitation Bohr radius has been reported to be in the range of 6.67-28.7 nm for CuO [24], which is near the size range of the synthesized particles obtained in this study.

For the synthesized CuO nanoparticles, the optical band gap energy (E_g) can be estimated using the Tauc's relation (Eq. 9) [2-3, 24-25]:

$$(\alpha h\nu)^n = B(h\nu - E_g) \qquad (9)$$

where α is the absorption coefficient, $h\nu$ is the photon energy, n equals either 1/2 for an indirect transition (indirect band gap semiconductors) or 2 for a direct transition (direct band gap semiconductors) and B is a material-dependent constant. The value of the absorption coefficient can be determined by Eq. 10 [2,24]:

$$\alpha = \frac{-1}{d}\ln\frac{I_t}{I_0} = \frac{A}{d\log e} \approx 2.303\frac{A}{d} \qquad (10)$$

where d is the thickness of the used cuvette (the sample thickness) and I_o and I_t are the intensities of incident and transmitted light, respectively. Here, A = log (I_o/I_t) is the absorbance which is obtained from the UV–V absorption spectra.

According to Eqs. 9 and 10, the band gap can be estimated from a plot of $(\alpha h\nu)^2$ versus photon energy ($h\nu$). By extrapolation of the linear regions in Fig. 8(b), E_g value of 2.5 eV for CuO nanoparticles was obtained which is much larger than the reported value for bulk CuO (E_g 1.2-1.9 eV). The blue-shift behavior of peak position in comparison with that of bulk CuO is attributed to the enhancement of the quantum confinement effect resulting from the decrease in the size of the [2-3,24].

4. Conclusions

This article introduced mechanochemical synthesis of CuO nanoparticles using copper hydroxide as the precursor. $Cu(OH)_2$ powder which were synthesized from $CuSO_4$ aqueous solution was milled in NaCl matrix to formulate CuO nanoparticles according to the equation below:

$$Cu\left(OH\right)_2 + 7NaCl\left(diluents\right) \rightarrow CuO + H_2O\left(g\right) + 7NaCl\left(diluents\right)$$
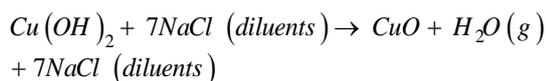
The results indicate that dehydration of Cu $(OH)_2$ into CuO was successfully achieved by mechanochemical process without subsequent annealing during the process. Also, 3h of milling is the optimum condition for mechanochemical synthesis of CuO nanoparticles.

It is also concluded that the conversion of a molar equivalent volume of Cu $(OH)_2$ into CuO would be associated with a volumetric contraction of approximately 56.45%. This value of volumetric contraction can lead to microstructural refinement during the mechanical dehydration.

E_g value of 2.5 eV for the CuO nanoparticles was obtained which is much larger than the reported value (E_g=1.2-1.9 eV) for bulk CuO.

References

[1]. Liu Q, Liu H, Liang Y, Xu Z, Yin G. Mate. Res. Bull. Vol 41 (2006) pp. 697-702.

[2]. Al-Gaashani R, Radimana S, Tabetc N, Razak Daud A. J. Alloy. Compd. Vol. 509 (2011) pp. 8761-9.

[3]. Hassan MS, Amna T, Yang O-B, El-Newehyd MH, Al-Deyab SS, Khil M-S. Colloid. Surface. B. Vol 97 (2012) pp. 201-6.

[4]. Wongpisutpaisan N, Charoonsuk P, Vittayakorn N, Pecharapa W., Energy Procedia. Vol 9 (2011) pp. 404-9.

[5]. Son DI, You CH, Kim TW., Appl. Surf. Sci. Vol 255 (2009) pp.8794-7.

[6]. Wang H, Xu J-Z, Zhu J-J, Chen H-Y., J. Cryst. Growth. Vol 244 (2002) pp. 88-94.

[7]. Han D, Yang H, Zhu C, Wang F., Powder Technol. Vol 185 (2008) pp. 286-90.

[8]. Jia W, Reitz E, Sun H, Zhang H, Lei Y., Mater. Lett. Vol 63 (2009) pp. 519-22.

[9]. Lu C, Qi L, Yang J, Zhang D, Wu N, Ma J., J. Physic. Chem. B. Vol 108 (2004) pp. 17825-31.

[10]. Song X, Sun S, Zhang W, Yu H, Fan W., J. Physic. Chem. B. Vol 108 (2004) pp. 5200-5.

[11]. Tsuzuki T, McCormick PG., Acta Mater. Vol 48 (2000) pp. 2795-801.

[12]. Tsuzuki T, McCormick PG., J. Mater. Sci. Vol 39 (2004) pp. 5143-6.

[13]. Yang H, Hu Y, Tang A, Jin S, Qiu G., J. Alloy. Compd. Vol 363 (2004) pp. 276-9.

[14]. Ao W, Li J, Yang H, Zeng X, Ma X., Powder. Technol. Vol 168 (2006) pp. 148-51.

[15]. Li YX, Chen WF, Zhou XZ, Gu ZY, Chen CM., Mater. Lett. Vol 59 (2005) pp. 48-52.

[16]. Tsuzuki T, Pirault E, McCormick PG., Nanostruct. Mater. Vol 11 (1999) pp. 125-31.

[17]. Li YX, Zhou XZ, Wang Y, You XZ., Mater. Lett. Vol 58 (2003) pp. 245-9.

[18]. Cudennec Y, Lecerf A., Solid. State. Sci. Vol 5 (2003) pp. 1471-4.

[19]. Aminzare M, Amoozegar Z, Sadrnezhaad SK., Mater. Res. Bull. Vol 47 (2012) pp. 3586-91.

[20]. Ding J, Tsuzuki, T, McCormick PG., J. Mater. Sci. Vol 34 (1999) pp. 5293-8.

[21]. Salari M, Rezaee M, Marashi SPH, Aboutalebi SH., Powder Technol. Vol 192 (2009) pp. 54-7.

[22]. Suryanarayana C., Prog. Mater. Sci. Vol 46 (2001) pp. 1-184.

[23]. Beygi H, Sajjadi SA, Zare M., Int. J. Adv. Manuf. Technol. Vol 70 (2014) pp. 1653-9.

[24]. Rehman S, Mumtaz A, Hasanain SK., J. Nanoparticle. Reasearch. Vol 13 (2011) pp. 2497-507.

[25]. Zhang X, Zhang D, Ni X, Zheng H., Solid. State. Electron. Vol 52 (2008) pp. 245-8.